

PROCEEDINGS OF SPIE

SPIEDigitalLibrary.org/conference-proceedings-of-spie

Restoration of time-of-flight (ToF) underwater images using TV regularization

Mack, Kevin, Athavale, Prashant, Jemison, William, Illig,
David, Rumbaugh, Luke, et al.

Kevin V. Mack, Prashant Athavale, William D. Jemison, David W. Illig, Luke K. Rumbaugh, Mahesh K. Banavar, Erik M. Bollt, "Restoration of time-of-flight (ToF) underwater images using TV regularization," Proc. SPIE 11752, Ocean Sensing and Monitoring XIII, 117520N (12 April 2021); doi: 10.1117/12.2588047

SPIE.

Event: SPIE Defense + Commercial Sensing, 2021, Online Only

Restoration of time-of-flight (ToF) underwater images using TV regularization

Kevin V. Mack^{a*}, Prashant Athavale^{a†}, William D. Jemison^{a*}, David W. Illig^b, Luke K. Rumbaugh^{c*}, Mahesh K. Banavar^{a*}, and Erik M. Boltt^{a*}

^aClarkson University, 8 Clarkson Ave, Potsdam, USA

^bNAWCAD, 22347 Cedar Point Rd, Patuxent River, USA

^cGrove City College, 100 Campus Dr, Grove City, USA

ABSTRACT

This paper investigates a total variation (TV) regularization image processing algorithm to restore underwater range images taken with a modified commercial time-of-flight (ToF) camera. The ToF camera illuminator was modified to support 532 nm flood illumination for underwater operation. This approach can produce high-resolution amplitude and range images while rejecting a significant amount of ambient light. However, scattering due to the water turbidity adversely impacts image quality by introducing high amounts of image noise and image blurring that affect both the amplitude and range images. The TV regularization algorithm is applied to experimental images taken in a small test tank in the presence of a scattering agent to simulate a range of practical turbidities. Algorithm details are provided, and baseline and processed images are presented. The processed images demonstrate image restoration that retains the downrange edge features of the object being imaged is possible for a range of practical turbidities.

Keywords: time-of-flight camera, underwater imaging, total variation, image restoration, scattering

1. INTRODUCTION

There is an increasing need for optical sensors that can improve situational awareness in a variety of underwater applications. These applications range from fundamental scientific research of marine organisms,^{1,2} to commercial applications such as bridge substructure³ and pipeline inspections,⁴ to underwater landscape exploration and mapping that is being enabled by the proliferation of unmanned underwater vehicles (UUV's).

There are many applications where high-resolution underwater images are desired. Much work is dedicated to the color correction of red-green-blue (RGB) images taken with traditional charge-coupled device (CCD) cameras. However, recent work has shown that color restoration requires *a priori* knowledge not only of the camera properties but also of the water conditions and/or dimensions of the object being imaged to guide the image reconstruction⁵ properly. This motivates using systems that can provide information about the true size and/or range of the object being imaged.

Underwater lidar and certain underwater imaging approaches can provide such spatial information. Underwater lidar approaches include hybrid lidar/radar,⁶ various line-scanning lidars,^{7–11} and commercial range-gated lidars.^{12–14} Imaging approaches include stereoscopic imaging.¹⁵ The authors recently proposed using commercial time-of-flight (ToF) cameras with modified illuminators to generate high-resolution underwater amplitude, and range images that provide both cross-range and downrange information.¹⁶ This paper aims to investigate the use of a TV regularization to improve the ToF images. TV regularization is an approach that has previously been applied to terrestrial ToF images to retain edge features.¹⁷ In this work, the TV regularization approach is applied to underwater range images to investigate the ability to retain downrange edge features.

The paper is organized as follows: Section 2 gives a brief overview of time-of-flight principles and how the range calculation is made. In Section 3, we describe the experimental set-up and signal processing approach. In Section 4, we present results for a range of turbidities.

Further author information: (Send correspondence to K.V. Mack: mackkv@clarkson.edu)

*Department of Electrical Engineering, [†]Department of Mathematics

2. TIME-OF-FLIGHT CAMERAS AND UNDERWATER OPERATIONAL CONSIDERATIONS

Commercial ToF cameras include range-gated systems and continuous wave (CW) modulated systems. Range-gated systems use pulsed illumination and time-gating to measure the photon time-of-flight over relatively short-range distances.^{13, 14} CW modulated systems use intensity modulation of a CW optical carrier to estimate the range from the modulation phase delay. Terrestrial autonomous vehicle navigation is a primary driver of ToF camera development. Terrestrial applications typically use eye-safe infrared optical wavelengths for the active illuminator, which are highly absorbed in water. Therefore, the use of a commercial time of flight camera for underwater use requires a wavelength modification of the active illuminator and an appropriate wavelength filter at the imaging chip. Blue-green wavelengths are often used for underwater work to minimize the absorption.

Underwater application of ToF cameras also requires an understanding of the underwater sensing environment which is challenging due to optical absorption and scattering. High signal absorption causes low signal-to-noise ratios, backscatter results in amplitude clutter resulting in loss of scene contrast, and forward-scattering causes image blurring. The signal attenuation due to both absorption and scattering may be estimated by Beer's Law,

$$A_{t0f} = P_{tr} \exp(-cz), \quad (1)$$

where A_{t0f} is the optical power measured by the camera, P_{tr} is the optical power transmitted into the channel, c is the beam attenuation coefficient with units of $1/m$, and z is the distance traveled through the channel with units of m . The dimensionless parameter cz is referred to as the number of attenuation lengths (AL) and can be used to compare different water conditions. Beer's Law is only accurate for sensors with collimated laser beam transmitters and narrow field of view receivers, as it assumes that the receiver cannot collect any scattered light. However, in high-scattering regimes, the amount of scattered light collected at the receiver may exceed the non-scattered signal. Nevertheless, Beer's Law is commonly used to estimate the amount of light collected by a variety of underwater optical sensor architectures.

2.1 Time-of-Flight Camera

The work described in this paper uses a commercial ESPROS DME 660 camera¹⁸ that was modified to modulate a 532 nm laser diode with a small angle diffuser. While some ToF cameras implement a thin film integrated infrared filter directly on the imaging chip, the DME 660 allows external filters and lens to be easily changed via an M-12 lens mount facilitating its use at 532 nm. A custom illuminator board was designed and interfaced to the camera using commercially available 532 nm laser diodes that flood illuminate the scene with modulated light. The wide beam illumination contributes to a larger common volume of overlap between the backscatter and the receiver than traditional line-scanning methods.

The DME 660 is a 12-bit camera with 320×240 pixels and can support frame rates up to 39 frames per second. Modulation frequencies up to 24 MHz are supported, which result in sub-centimeter range resolution. Distance is calculated by first computing the phase delay between the transmitted modulation waveform and the waveform received from the object being imaged. For each range calculation four differential correlation samples (DCS) labelled $\mathbf{Q}_i, i \in \{0, 1, 2, 3\}$ are used at each pixel. Though only two DCS measurements are needed to compute a phase offset estimate, the camera uses two extra samples to help with noise and ambient light rejection. The DCS values are used to compute the amplitude of the signal and the phase offset, which is proportional to the round-trip time and, therefore, the distance traveled by the signal. Figure 1 shows the basic modulation waveform.¹⁸ The phase offset due to the delay between the transmitted waveform and the received waveform is computed as shown below.

$$\phi_{t0f} = \arctan \left(\frac{\mathbf{Q}_2 - \mathbf{Q}_0}{\mathbf{Q}_3 - \mathbf{Q}_1} \right), \quad (2)$$

The distance and amplitude for each measurement are given below,

$$\mathbf{d}_{t0f} = \frac{v}{2} \frac{1}{2\pi f_{mod}} \left(\pi + \phi_{t0f} \right) + d_{offset}, \quad (3)$$

$$\mathbf{A}_{t0f} = \sqrt{\left(\frac{\mathbf{Q}_2 - \mathbf{Q}_0}{2} \right)^2 + \left(\frac{\mathbf{Q}_3 - \mathbf{Q}_1}{2} \right)^2}. \quad (4)$$

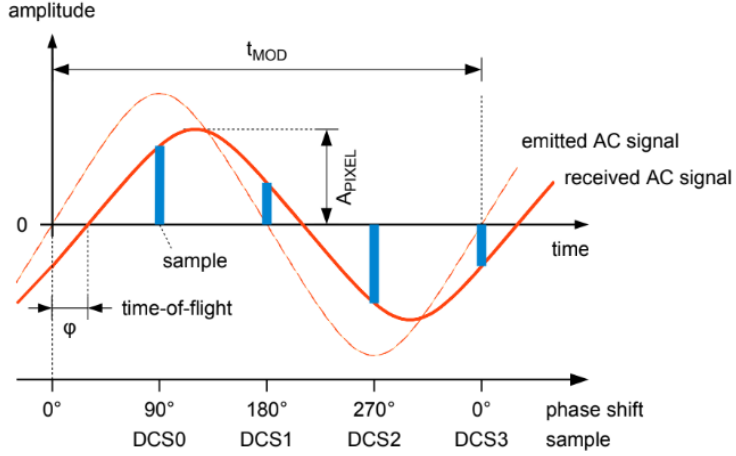


Figure 1: Illustration of the concept of modulation phase measurements by a CW ToF system.¹⁸ The ToF camera captures four samples of the received modulation phase, each with 90° of separation.

3. METHODS

This section describes the experimental setup and approach taken to investigate the use of the TV regularization algorithm to denoise and deblur the underwater ToF range images. Image data was obtained from the modified Espros DME 660 ToF camera described in our previous work.¹⁶ Data were collected in a small test tank, and Maalox was used as a scattering agent to vary the turbidity, simulating scattering properties of actual ocean waters.¹⁹ The turbidity was measured with a Sea-Bird Scientific c-star transmissometer. A LEGO® object located at a fixed 0.7 m standoff range was used as a diffuse target. The LEGO® object was constructed to provide discrete 2 cm jumps in downrange features that were on the order of the range resolution of the ToF camera. A picture of the experimental setup and LEGO® target are shown in Figure 2.

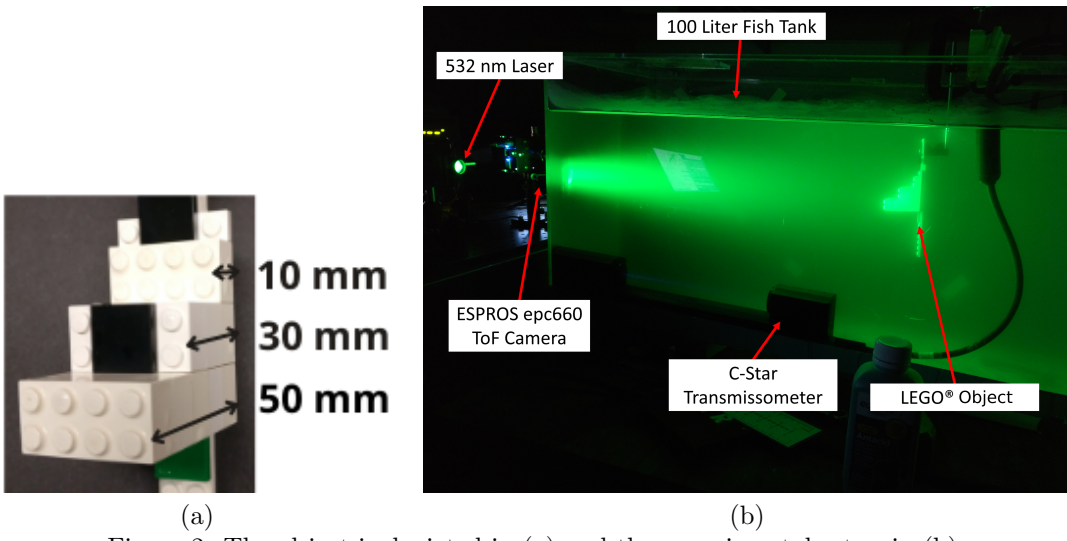


Figure 2: The object is depicted in (a) and the experimental setup in (b).

The baseline images used in this work were taken from the standard camera configuration. The dataset contains four DCS images consisting of 12-bit signed integer values, $\mathbf{Q}_i(x, y) \in [-2047, 2048]$ from each hardware demodulation channel. A modulation frequency of 24 MHz was used to achieve the best range resolution, and an integration time of 4000 μs was used as a baseline. The lens was focused on the object in clear water and thus constitutes some *a priori* knowledge about the object range. Four DCS values were used per pixel, which

are then computed to a range given by Eq. (3).

3.1 Preprocessing

Several preprocessing steps were conducted before applying the TV regularization algorithm. It is noted that in an underwater application, there may well be many pixels in a given frame that do not contain object information. However, they may contain significant returns due to backscatter. Likewise, in highly turbid conditions, backscatter may dominate a section of the scene that contains the object of interest. The work by Frank *et al.*²⁰ showed that Eq. (4) could be used as a biased estimator of the phase variance, thus helping determine confidence of the measured phase and range. In traditional in-air sensing, this allows for the ability to put a bound on distance resolution and error performance based only on measurable factors. However, in low signal conditions, fixed-pattern noise (FPN) dominates the received signal, causing the amplitude not to model the phase variance closely.²¹

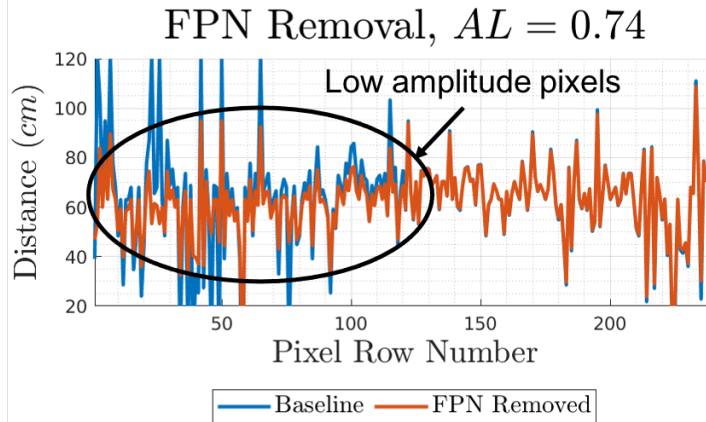


Figure 3: The FPN noise is removed as a preprocessing step. The pixels in rows 0 – 125 display low amplitude data, and thus a wider disparity between the baseline and preprocessed data than the subsequent rows- this behaviour is expected in the low amplitude pixels where FPN dominates.^{20,21}

To address FPN, we first applied the approach of Frank and Georgiev.^{20,21} This was accomplished through a series of calibration measurements.²¹ The removal of FPN is done to each set of DCS frames, which are then used to compute amplitude and phase. The results of this step are shown in Figure 3. While this step is intended to improve the signal-to-noise ratio, it does not address clutter and blurring problems associated with scattering. In the next section, we describe the use of TV regularization to restore the range image without blurring the edge features.

3.2 Total Variation Regularization for Underwater ToF Cameras

TV regularization has been used successfully to reconstruct noisy images while retaining edge features and is based on the seminal work by Rudin, Osher, and Fatemi (ROF).²² Since the original work, an enormous body of research has been done to improve the ROF variational approach to image denoising, both in analysis and computation. In this work, we take the formulation from Chan *et al.*,²³ and apply this to the range images to investigate its ability to retain downrange features in the presence of backscatter and forward scatter. Although neither of these physical phenomena is technically noise processes, we assume that they can be approximated as noise sources for the TV regularization model.

Thus, we receive a noisy image, \mathbf{b} , that includes forward scatter and backscatter and attempt to denoise and recover the original image \mathbf{u} . Using the notation from Chambolle,^{24,25} we can write the discrete denoising problem as,

$$\min_{\mathbf{u} \in X} \|\nabla \mathbf{u}\|_1 + \lambda \|\mathbf{u} - \mathbf{b}\|_1, \quad (5)$$

where \mathbf{u} is the solution or denoised image, X is the finite dimensional vector space that represents the image domain, $\nabla(\cdot)$ represents the discrete fixed-point derivative, and λ is the regularization parameter. The numerical

solution is found using the popular primal-dual algorithm for L_1 problems, once again we refer to Chambolle *et al.*^{24,25}

This formulation is used over ROF for its inherent invariance to image contrast, which implies that it may be more appropriate for low-contrast datasets, such as those expected from underwater ToF camera images. We also note that the variational methods derived by Lenzen *et al.*¹⁷ for ToF data use the amplitude given in Eq. (4) to weight the fidelity term in their objective function - this is based on the ToF noise model derived by Frank *et al.*²⁰ The result in terrestrial applications is an improvement in the denoising - however, we cannot use this formulation due to high amplitude backscatter in the high turbidity underwater environment. For now, we take the TV_{L_1} formulation as is and leave the adaptation to underwater backscatter-induced clutter to future work. The remaining obstacle in solving Eq. (5) is determining the parameter λ .

3.3 Parameter Selection

The scalar regularization parameter, λ , balances the amount of smoothing with the amount of signal left in the solution. While algorithms exist to optimize the choice of λ , in this work, we explore a small set of possible values of λ , as shown in Figure 4. Figure 4 plots the downrange profile slice of the LEGO® object used in our experiments. The dashed curve is the ground truth corresponding to the physical dimensions of the object, while the other curves show the TV regularization reconstruction achieved using five values of λ . When λ is too small, it results in over smoothing of the solution. However, when the parameter is too large, too much noise is left in the solution. We aim to select the best balance of these features in order to restore the distance image. Based on a qualitative assessment, we set $\lambda = 0.5$ for this work. This value worked well over a large range of conditions. Future work will address a more rigorous selection of the regularization parameter.

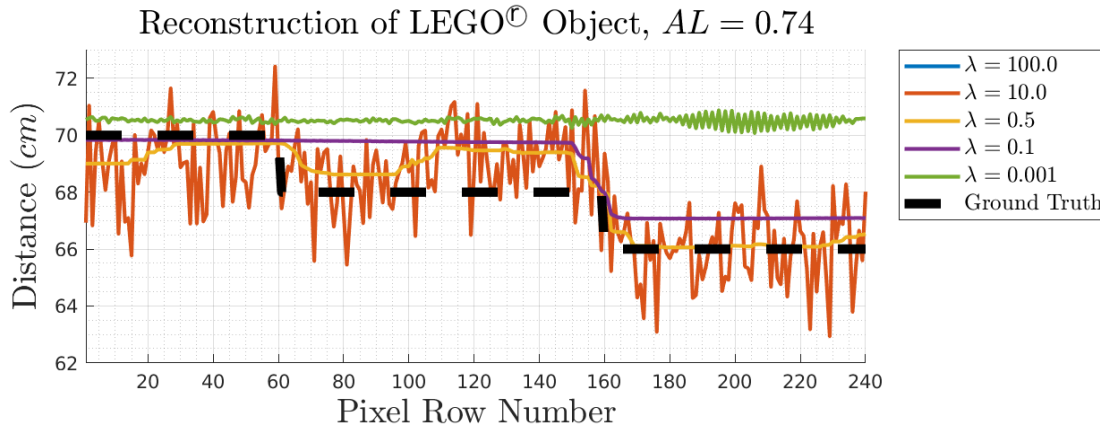


Figure 4: Effect of the regularization parameter on the solution. A lower λ results in more smoothing, while a higher value results in more noise. The optimal λ is one that balances the smoothing and fidelity terms in (5). In the figure, $\lambda = 0.001$ and $\lambda = 0.1$ depict oversmoothing, while $\lambda = 10.0$ and $\lambda = 100.0$ result in too much noise- $\lambda = 0.5$ is selected as the optimal parameter in this subset.

4. RESULTS

Figure 5 shows the results of the TV regularization algorithm for four different turbidities that correspond to attenuation lengths of 0.74, 3.67, 5.37, and 6.99. A TV regularization parameter of $\lambda = 0.5$ is used in all cases. The left column shows amplitude images taken at each condition, with the vertical red line showing the location of the downrange slice that is provided for each case in the right column. The range slice chosen has three distinct surfaces that lie at different depths, demonstrating the camera's ability to measure fine range features on an underwater object. Each range plot shows the ground truth corresponding to the measured physical dimension of the object, the range slice computed from the baseline ToF camera image, and the range slice computed with TV regularization. The TV regularization results improved the range measurement in all cases: TV regularization successfully denoised the range data while maintaining the approximate object structure.

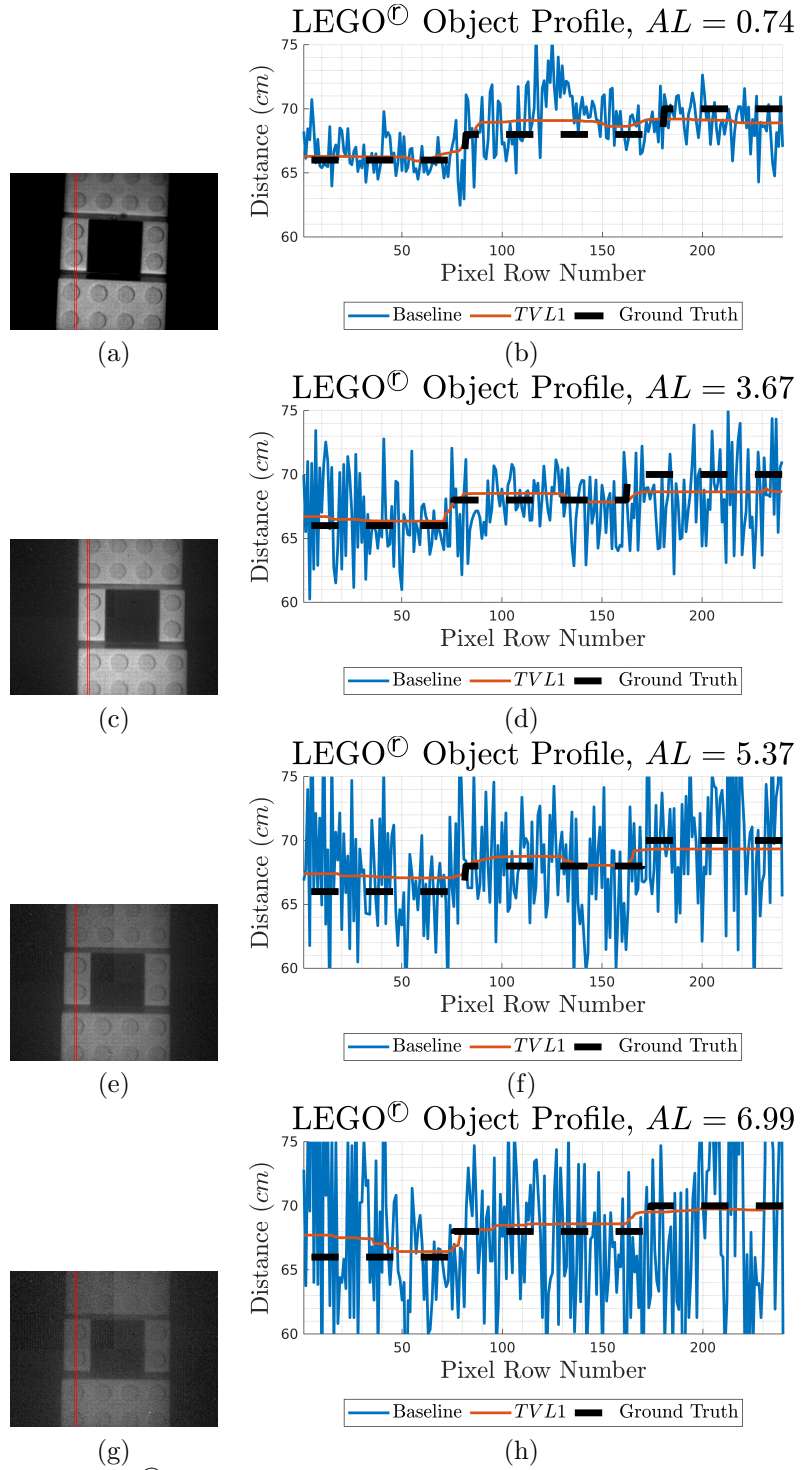


Figure 5: A profile of the LEGO® object face. The first column depicts the amplitude image at the specified turbidity level, as well as the column that is chosen to represent the object profile. The second column of figures is the profile of the specified column. The object face has three distinct surface distances at 66 cm, 68 cm, and 70 cm. The baseline and TV profiles are compared to the ground truth for various levels of water clarity, given by (a)(b) $AL = 0.74$, (c)(d) $AL = 3.67$, (e)(f) $AL = 5.37$, and (g)(h) $AL = 6.99$.

5. CONCLUSION

We investigated the TV regularization algorithm for reconstructing range images taken from a commercial ToF camera modified for underwater use in this work. The algorithm provided good qualitative performance in improving downrange measurement accuracy over a wide range of turbidities. Future work will aim to quantify the accuracy improvement of the algorithm, automate the selection of the TV regularization parameter, and further develop algorithm modifications required to address the unique challenges presented in the underwater environment.

6. ACKNOWLEDGEMENTS

This work is supported by the Office of Naval Research grant N00014-18-1-2291. Any opinions, findings, and conclusions, or recommendations expressed in this material are those of the authors and do not necessarily reflect the views of the Office of Naval Research.

REFERENCES

- [1] Mariani, P., "Jellyfish Identification Software for Underwater Laser Cameras (JTRACK)," *Research Ideas and Outcomes* **4**, e24716 (Feb. 2018). Publisher: Pensoft Publishers.
- [2] Dubrovinskaya, E., Dalgleish, F., Ouyang, B., and Casari, P., "Underwater LiDAR Signal Processing for Enhanced Detection and Localization of Marine Life," in [2018 OCEANS - MTS/IEEE Kobe Techno-Oceans (OTO)], 1–8, IEEE, Kobe (May 2018).
- [3] Shen, J., Forsyth, R., and Kilgore, R., "Underwater Inspection of Bridge Substructures Using Imaging Technology," (June 2018). Number: FHWA-HIF-18-049.
- [4] McLeod, D., Jacobson, J., Hardy, M., and Embry, C., "Autonomous inspection using an underwater 3D LiDAR," in [2013 OCEANS - San Diego], 1–8 (Sept. 2013). ISSN: 0197-7385.
- [5] Rzhanov, Y. and Lowell, K., "On the (im)possibility of color reconstruction in underwater images," in [OCEANS 2019 MTS/IEEE SEATTLE], 1–4 (Oct. 2019). ISSN: 0197-7385.
- [6] Mullen, L. J. and Contarino, V. M., "Hybrid LIDAR-radar: Seeing through the scatter," *IEEE Microwave Magazine* **1**, 42–48 (Sept. 2000).
- [7] Ouyang, B., Dalgleish, F. R., Caimi, F. M., Vuorenkoski, A. K., Giddings, T. E., and Shirron, J. J., "Image enhancement for underwater pulsed laser line scan imaging system," in [Ocean Sensing and Monitoring IV], **8372**, 83720R, International Society for Optics and Photonics (June 2012).
- [8] Ouyang, B., Dalgleish, F. R., Caimi, F. M., Giddings, T. E., Shirron, J., Vuorenkoski, A. K., Britton, W., Metzger, B., Ramos, B., and Nootz, G., "Compressive sensing underwater laser serial imaging system," *Journal of Electronic Imaging* **22**, 021010 (Mar. 2013). Publisher: International Society for Optics and Photonics.
- [9] Laux, A., Mullen, L., Perez, P., and Zege, E., "Underwater laser range finder," in [Ocean Sensing and Monitoring IV], **8372**, 83721B, International Society for Optics and Photonics (June 2012).
- [10] Rumbaugh, L. K., Boltt, E. M., Jemison, W. D., and Li, Y., "A 532 nm chaotic lidar transmitter for high resolution underwater ranging and imaging," in [2013 OCEANS - San Diego], 1–6 (Sept. 2013). ISSN: 0197-7385.
- [11] Rumbaugh, L. K., Dunn, K. J., Boltt, E. M., Cochenour, B., and Jemison, W. D., "An underwater chaotic lidar sensor based on synchronized blue laser diodes," in [Ocean Sensing and Monitoring VIII], **9827**, 98270I, International Society for Optics and Photonics (May 2016).
- [12] Massot-Campos, M. and Oliver-Codina, G., "Optical Sensors and Methods for Underwater 3D Reconstruction," *Sensors (Basel, Switzerland)* **15**, 31525–31557 (Dec. 2015).
- [13] Cametti, E., Dell'Acqua, S., Farinello, P., Piccinno, G., and Reali, G., "UTOFIA project: A novel MOPA laser source for a compact, cost-effective system for underwater range-gated imaging," in [18th Italian National Conference on Photonic Technologies (Fotonica 2016)], 1–4 (June 2016).

- [14] Driewer, A., Abrosimov, I., Alexander, J., Benger, M., O'Farrell, M., Haugholt, K. H., Softley, C., Thielemann, J. T., Thorstensen, J., and Yates, C., "UTOFIA: an underwater time-of-flight image acquisition system," in [*Electro-Optical Remote Sensing XI*], **10434**, 1043404, International Society for Optics and Photonics (Oct. 2017).
- [15] Jaffe, J. S., "Underwater Optical Imaging: The Past, the Present, and the Prospects," *IEEE Journal of Oceanic Engineering* **40**, 683–700 (July 2015).
- [16] Mack, K. V., Jemison, W. D., Rumbaugh, L. K., Illig, D. W., and Banavar, M. K., "Time-of-Flight (ToF) Cameras for Underwater Situational Awareness," in [*OCEANS 2019 MTS/IEEE SEATTLE*], 1–5 (Oct. 2019). ISSN: 0197-7385.
- [17] Lenzen, F., Kim, K. I., Schäfer, H., Nair, R., Meister, S., Becker, F., Garbe, C. S., and Theobalt, C., "Denoising Strategies for Time-of-Flight Data," in [*Time-of-Flight and Depth Imaging. Sensors, Algorithms, and Applications: Dagstuhl 2012 Seminar on Time-of-Flight Imaging and GCPR 2013 Workshop on Imaging New Modalities*], Grzegorzek, M., Theobalt, C., Koch, R., and Kolb, A., eds., *Lecture Notes in Computer Science*, 25–45, Springer, Berlin, Heidelberg (2013).
- [18] "ESPROS Photonics Corporation - Welcome to ESPROS."
- [19] Laux, A., Billmers, R., Mullen, L., Concannon, B., Davis, J., Prentice, J., and Contarino, V., "The a, b, c's of oceanographic lidar predictions: a significant step toward closing the loop between theory and experiment," *Journal of Modern Optics* **49**(3/4), 439–451 (2002).
- [20] Frank, M., Plaue, M., and Hamprecht, F. A., "Denoising of continuous-wave time-of-flight depth images using confidence measures," *Optical Engineering* **48**, 077003 (July 2009). Publisher: International Society for Optics and Photonics.
- [21] Georgiev, M., Bregovic, R., and Gotchev, A., "Fixed-Pattern Noise Modeling and Removal in Time-of-Flight Sensing," *IEEE Transactions on Instrumentation and Measurement* **65**, 1–13 (Nov. 2015).
- [22] Rudin, L. I., Osher, S., and Fatemi, E., "Nonlinear total variation based noise removal algorithms," *Physica D: Nonlinear Phenomena* **60**, 259–268 (Nov. 1992).
- [23] Chan, T. F. and Esedoḡlu, S., "Aspects of Total Variation Regularized L1 Function Approximation," *SIAM Journal on Applied Mathematics* **65**(5), 1817–1837 (2005). Publisher: Society for Industrial and Applied Mathematics.
- [24] Chambolle, A. and Pock, T., "A first-order primal-dual algorithm for convex problems with applications to imaging," (2010).
- [25] Chambolle, A., Novaga, M., Cremers, D., and Pock, T., "An introduction to total variation for image analysis," in [*Theoretical Foundations and Numerical Methods for Sparse Recovery*, De Gruyter], (2010).